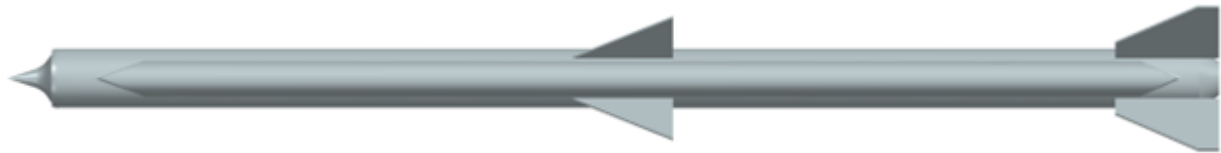


AE 721 Report 10: RAIDER Weapon System Design



Authors: James Wall, Niels Braaten, Sap
Dutta, Charlie Platt, Isaac Larsen

Instructor: Dr. Ron Barrett



Department of Aerospace Engineering

December 3, 2023

Acknowledgment

Thank you to money, because that is the sole desire that drives college students.

And to cool car makers...

So we can spend that money on the cool cars.

Thank you to money and cool cars.

Table of Contents

Acknowledgment.....	ii
List of Symbols.....	v
1 Previous RAIDER Work.....	1
2 General RAIDER Layout.....	4
3 Flight Assumptions and Mission Profile.....	5
4 RAIDER Design for Mach 4 at Burnout Altitude, Cruise Initiation Point.....	7
4.1 Determination of Required Thrust at Cruise Initiation Point.....	7
4.2 Assumptions.....	7
4.3 Calculate A_0 and A_{IT}	7
4.4 Combustor Inlet Mach Number and Area, Exit Mach Number, and Pressure.....	9
4.5 Speed of Sound in Combustion Chamber.....	12
4.6 Combustion Speed, V_4	12
4.7 Combustion Chamber Length Calculation, L_c	12
4.8 Throat Area Determination.....	13
4.9 Expansion Bell/ Nozzle Design.....	13
4.10 Engine Thrust and I_{sp}	14
5 Design Iteration and Optimization.....	16
5.1 Iteration Process.....	16
5.2 Iteration 1.....	17
5.3 Iteration 2.....	17
5.4 Iteration 3.....	17
5.5 Iteration 4.....	18
5.6 Iteration 5.....	18
5.7 Materials.....	18
6 Final RAIDER Weapon CAD Figures.....	21
6.1 Four-View.....	21
6.2 Full-Color Cutaway.....	24
6.3 Fully Collapsed/ Stowed.....	25
6.4 Separated.....	26
6.5 Dash and Terminal Configuration.....	27

7	Conclusions and Recommendations.....	29
7.1	Conclusions.....	29
7.2	Recommendations.....	30
7.3	Section Responsibilities.....	31
	References	

List of Symbols

<u>Symbol</u>	<u>Description</u>	<u>Units</u>
a	Speed of Sound	Ft/s (m/s)
A_e	Effective Area	in^2 (m^2)
A_0	Inlet Area	in^2 (m^2)
A_{IT}	Inlet Throat Area	in^2 (m^2)
AR	Aspect Ratio	(~)
c_{mac}	Mean Aerodynamic Chord	in (m)
c^*	Characteristic Velocity	ft/s (m/s)
C_D	Coefficient of Drag	(~)
C_{D0}	Zero-Lift Drag Coefficient	(~)
C_L	Coefficient of Lift	(~)
$C_{L \text{ cruise}}$	Coefficient of Lift at Cruise	(~)
C_N	Coefficient of Normal Force	(~)
C_p	Isobaric Specific Heat	BTU/lbm/R (J/kg/K)
d	Diameter	Ft (m)
D	Drag	Lbf (N)
E	Elastic Modulus	Psi (Pa)
f/a	Fuel-Air Ratio	(~)
g	Gravity	ft/s (m/s)
h	Altitude	Ft (m)
Hf	Heat of Combustion	BTU/lbm (J)
I_{sp}	Specific Impulse	sec
l	Missile Length	in (m)
l/d	Body Fineness Ratio	(~)
l_N	Nose Length	in (m)
l_N/d	Nose Fineness Ratio	(~)
L	Lift	Lbf (N)
L_C	Combustion Chamber Length	ft (m)
L/D	Lift to Drag Ratio	(~)

List of Symbols Continued

<u>Symbol</u>	<u>Description</u>	<u>Units</u>
m_{air}	Mass Flow of Air	lbm/s (kg/s)
m_{tot}	Mass Flow Total	lbm/s (kg/s)
M	Mach Number	(~)
M_{IE}	Inlet Start Mach Number	(~)
N	Normal Force	Lbf (N)
p	Pressure	Psi (Pa)
q	Dynamic Pressure	Psf (Kg/m ³)
R	Gas Constant	ft-lbf/slug-R (J/K-mol)
S_{Ref}	Reference Area	Ft ² (m ²)
T	Temperature	R (K)
T	Thrust	Lbf (N)
t	Thickness	in (m)
t_{comb}	Typical Combustion Time	s
V	Velocity	ft/s (m/s)
W	Weight	Lbm (N)
W_{Fuel}	Fuel Weight	Lbm (N)
$W_{Takeoff}$	Takeoff Weight	Lbm (N)
x_{AC}	Aerodynamic Center Location	in (m)
x_{CG}	Center of Gravity Location	in (m)
x_{HL}	Hinge Line Location	in (m)

Greek Symbols

α	Angle of Attack	Deg. or Rad
α_{Cruise}	Angle of Attack at Cruise	Deg. or Rad
γ	Ratio of Specific Heats	(~)
δ	Control Surface Deflection	Deg. Or Rad
ε	Nozzle Expansion Ratio	(~)

Greek Symbols Cont.

ρDensitySlugs/ft ³ (Kg/m ³)
ρ_{Cruise}Density at CruiseSlugs/ft ³ (Kg/m ³)
ϕRoll AngleDeg. or Rad
φRoll AngleDeg. or Rad
ω_{BB}First Mode Body Bending FrequencyDeg./s or Rad/s

Subscripts

AirAir is being Measured---
ACAerodynamic Center---
BBody---
BBBody Bending---
BTBoattail---
combCombustion---
CCombustion Chamber---
CGCenter of Gravity---
CruiseCruise Altitude---
iIteration---
eExit---
FFlare---
HLHinge Line---
IEInlet Start---
ITInlet Throat---
macMean Aerodynamic Chord---
NNose---
RefBody Reference---
spSpecific---
tTotal---
totTotal---
0Initial Condition---

Acronyms

A-A	Air-to-Air
A.C.....	Aerodynamic Center
AIM.....	Air Intercept Missile
AMRAAM.....	Advanced Medium-Range Air-to-Air Missile
AMRAAM-ER.....	Advanced Medium-Range Air-to-Air Missile Extended Range
BVR	Beyond Visual Range
C/D.....	Convergent Divergent
D-3	Delta-3
ECCM.....	Electronic Counter-Countermeasures
ER	Extended Range
FL	Flight Level
F3R	Form, Fit, Function Refresh
F/A	Fighter/Attacker
GPS	Global Positioning System
HE	High Explosive
HL	Hinge Line
HM.....	Hinge Moment
RAIDER	Ram Air Inflated Ducted Eccentric Ramjet
RDT&E.....	Research, Development, Test, & Evaluation
SOTA.....	State-of-the-Art
US	United States
USD	United States Dollars
2-D	Two-Dimensional

1 Previous RAIDER Work

The Ram Air Inflated Ducted Eccentric Ramjet (RAIDER) configuration of the AIM-120 AMRAAM has been investigated by the authors. This investigation consisted of benchmarking the AIM-120D-3 so the RAIDER configuration could include 5th-generation fighter integration, tube-launching capability, efficiency, and dimensional savings with unaltered salience. The authors researched the state-of-the-art AIM-120: the AIM-120D-3, as it is the most modern AMRAAM with public data available. The AIM-120D-3 has improved seeker capabilities, guidance, control surfaces, propulsion systems, warhead and launcher systems compared to the AIM-120C variants and was first live-fired in December 2020.

Once the research for the AIM-120D-3 was complete, the authors benchmarked the AIM-120 performance without wings or fins. The D/CD was related with dynamic pressure showing the increase in drag at high Mach numbers and the reduction at higher altitudes. The body first bending mode frequency is related to the body fineness ratio and E_t/W with increasing fineness ratio leading to a lower bending frequency and a smaller E_t/W also leading to a lower bending frequency. The CD_0 of the body in coast and powered were compared with the coast condition having higher zero-lift drag coefficient at all Mach numbers. The $C_{D0_bodywave}$ was then related to the nose fineness ratio and found at different Mach numbers, this showed that having a higher fineness ratio leads to lower body wave drag coefficient. The boattail effect is determined for the AIM-120 and the Fleeman example finding the CD_0 against Mach number in coast and powered modes.

The body normal force coefficient is related to the aspect ratio and change based on the angle of attack. This was graphed to show the effects of a higher aspect ratio leading to a higher normal force coefficient, especially at large angle of attack. The body lift-to-drag ratio is related to the aspect ratio, fineness ratio and angle of attack; the results were plotted by different configurations with the AIM-120 being a low-drag, high-fineness missile. The body lift-to-drag ratio is related with dynamic pressure and graphed for different altitudes to find that higher dynamic pressures lead to lower lift to drag ratios. The L/D found for the AIM-120 was low at 0.0905 and the volumetric efficiency was also low at 3.22. The body aerodynamic center is predicted for the AIM-120 by the angle of attack, nose length and aft body length where the AIM-120 distance to body aerodynamic center/length of the nose is 7.6. The flare stabilizer effect increases the static stability of the AIM-120 with a 10-degree half angle flare changing the diameter of the missile in at the aft portion to 7.8 inches. The flare would start where the boattail normally starts and end when the boattail normally ends. The aerodynamic center for the body with the addition of the flare is found at 39.5 inches from the nose of the missile based on slender body theory.

The normal force was predicted for the missile from angle of attack, using slender wing theory and linear wing theory, by summing the normal forces from the wing, body, and tail. The aerodynamic center for the planar surfaces was predicted for the AIM-120 wing and tail at low angle of attack and supersonic Mach number. This equation found the shift of the

aerodynamic center from 0.25 at subsonic speeds to near 0.5 at supersonic speeds. The hinge moment is predicted by the normal force of the wing, the aerodynamic center, and the hinge line at different effective angle of attack. The surface skin friction drag is predicted by the zero-lift surface skin friction drag using the half-wetted surface area at different Mach numbers. The surface wave drag is used with the surface skin friction drag to find the planar surface drag; this is found with the Mach number perpendicular to the leading edge showing that the wave drag of the AIM-120 is lower with a swept leading edge and a small section angle. The wing lift-to-drag ratio with respect to wing local angle of attack is found by the normal forces and the angle of attack with a large peak at low angle of attack then a gradual decrease as alpha increases.

The surface planform geometry and alternatives were covered which included lattice fins for control at the tail; the AA-12 was the basis as it has a similar length and diameter to the AIM-120 for which 10.5 inch by 4.5-inch fins with 1.5-inch square cells was chosen and the choked flow region analyzed.

The tail area of the AIM-120 was sized using the center of gravity without fuel to achieve a neutral static margin. The aerodynamic configuration buildup was done at Mach 2 and Mach 4 by adding the normal force coefficient of the body, wing, and tail. At both flight conditions the body is the largest contributor to the normal force, while at low alpha the normal force coefficient was low with the high alpha normal force coefficient much larger at both Mach 2 and Mach 4 with the Mach 4 normal forces being lower.

The reverse engineering of the AIM-120 was started with the baseline missile data from research and analysis. The design mission profile was constructed for the AIM-120 with the launch, acceleration, dash out Mach 4, terminal maneuver Mach 4, and impact. The payload range diagram showed the maximum range at 99 miles. The weight of the propellant is found from the stations 15-70 which gives a fuel tank length of 55 inches, this leads to a fuel volume of 1,900 in³ and a weight of 116 lbs for the AIM-120D. The specific impulse and TSFC are found from the delivered specific impulse graph assuming a high energy propellant leading to a specific impulse of 265 seconds and a TSFC of 13.6 lbf/lbf-hr. The time of flight with live engine estimation was estimated with the weight, thrust, and TSFC to be 7.812 seconds and this was used to find the weight flow rate of the fuel to be 13.85 lbf/s.

The updated mission profile was then constructed with the derived values from previous sections. The mission L/D was found with the thrust and weight assuming induced drag is negligible, and wave drag dominates leading to a L/D of 4.84. The empty weight to launch weight ratio was calculated with the launch weight without the propellant and warhead weight divided by the launch weight to give a ratio of 0.55. The lift and drag coefficients were found with respect to angle of attack at different Mach numbers. The angle of attack was found where the cruise L/D was 4.84 to be 9.2 degrees. The lift coefficient at cruise was found for this same L/D to be 1.46. The cruise midpoint air density was found assuming 50% fuel load with a density of 0.000103 slug/ft³. The mid-cruise point altitude for standard atmosphere is at an altitude of 76,000 ft to give a speed of sound of 968 ft/s at this altitude. The updated mission profile was then created with the mid-point cruise details found in previous sections.

The proverse engineering of the AIM-120 RAIDER began with the table of all known aerodynamic and inertial information from the previous section and Janes. The RIM-8 Talos missile cross sectional inlet duct area was used to approximate the RAIDER ramjet inlet duct area. The RAIDER variant differs by having the ducts on either side of the missile in a “plus” configuration with the wing and tail fins in the “x” configuration, seen below in Figure 1-1.

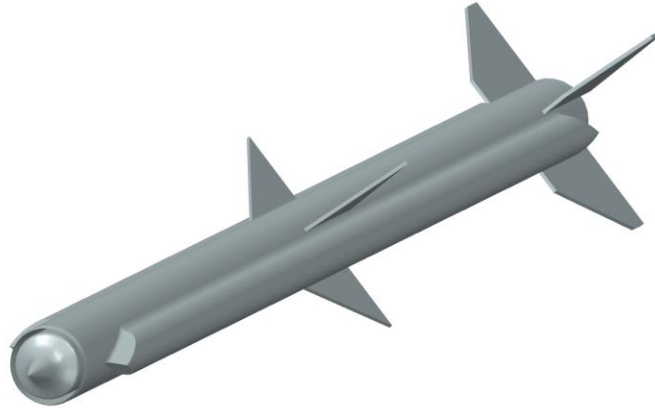


FIGURE 1-1: AIM-120 RAIDER CAD [1]

The individual duct cross section area was calculated to be 5.73 in² and the inner missile cone has a diameter of 5.8 in; the added ducts increase the hydraulic diameter of the AIM-120 RAIDER to be 7.975 in. The tube-launched variant was optimized by reducing volume while preserving the performance of the missile, particularly the range, seeker, and warhead weight. The RAIDER is determined to be 65% of the geometric size of the AIM-120 and decreased 113 pounds. The AIM-120 RAIDER CAD drawing was made to show the new configuration along with a bill of materials to be ordered, the components to be 3D printed, and the method of assembly [1]. The finished AIM-120 RAIDER model is seen below in Figure 1-2.



FIGURE 1-2: AIM-120 RAIDER [2]

2 General RAIDER Layout

This section of the report covers the general RAIDER layout. Shown below in Figure 2-1 is a not-to-scale line drawing, and a 3-D internal cutout drawing of the propulsion layout of the AIM-120 AMRAAM RAIDER variant is shown in Figure 2-2. Figure 2-2 includes the quasi-isentropic inlet, side ducts, combustor inlet throat, combustion chamber in the tail stock, flameholders and a converging-diverging nozzle. The different numbered parts separate the main sections of the propulsion system.

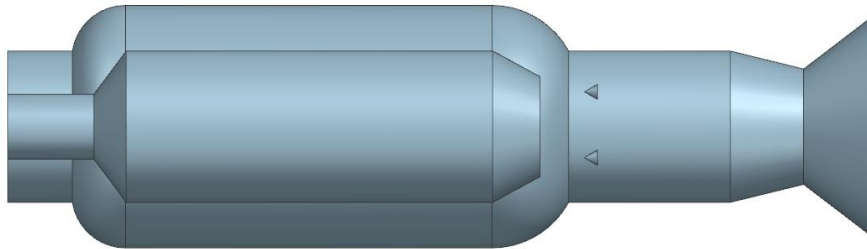


FIGURE 2-1: GENERAL RAIDER OUTER MOLD LINE

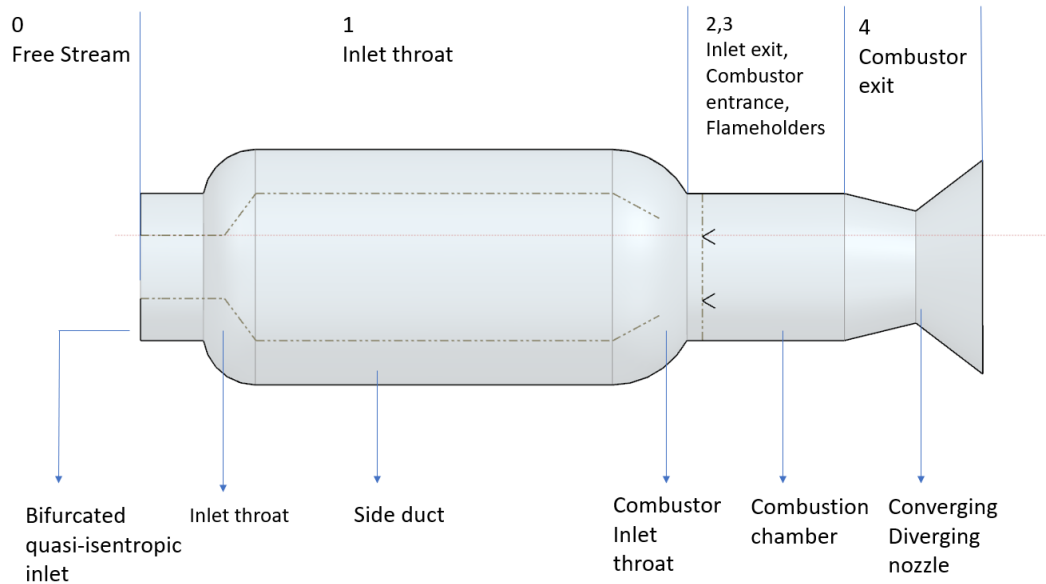


FIGURE 2-2: LABELED RAIDER LAYOUT

3 Flight Assumptions and Mission Profile

This section of the report details the flight assumptions and mission profile of the AIM-120 missile. The authors assume that the AIM-120 missile will be reliant upon a rocket launch to attain an altitude of at least 80,000 feet with rocket motor burnout at Mach 4 before RAIDER engagement, per instruction of advisor Dr. Ron Barrett. From previous work in Section 14 of Report 6, the following mission profiles and altitude calculations are obtained [1]:

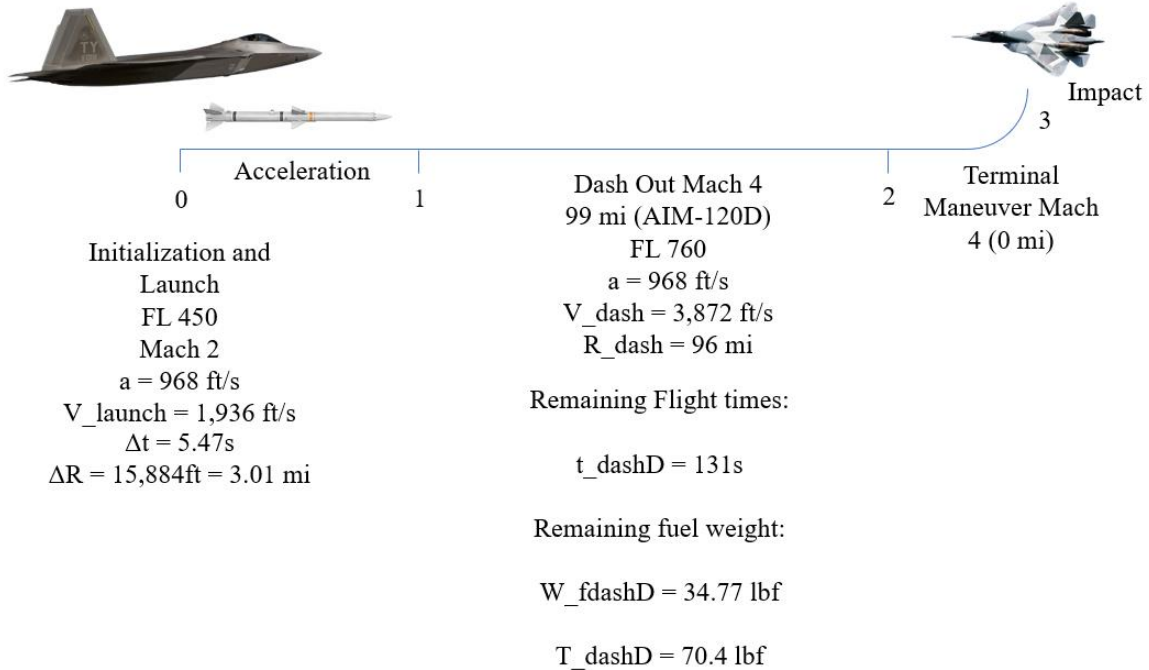


FIGURE 3-1: AIM-120 MISSION PROFILE [1]

An initial launch from an aircraft at an altitude of 45,000 ft is assumed at a speed of Mach 2. The lift coefficient (C_L) at cruise ($C_{L_{cruise}}$) is found where the cruise L/D is 4.84 on the Mach 4 graph shown in Figure 14.10.8 in Report 6. This figure is shown below as Figure 3-2 [1].

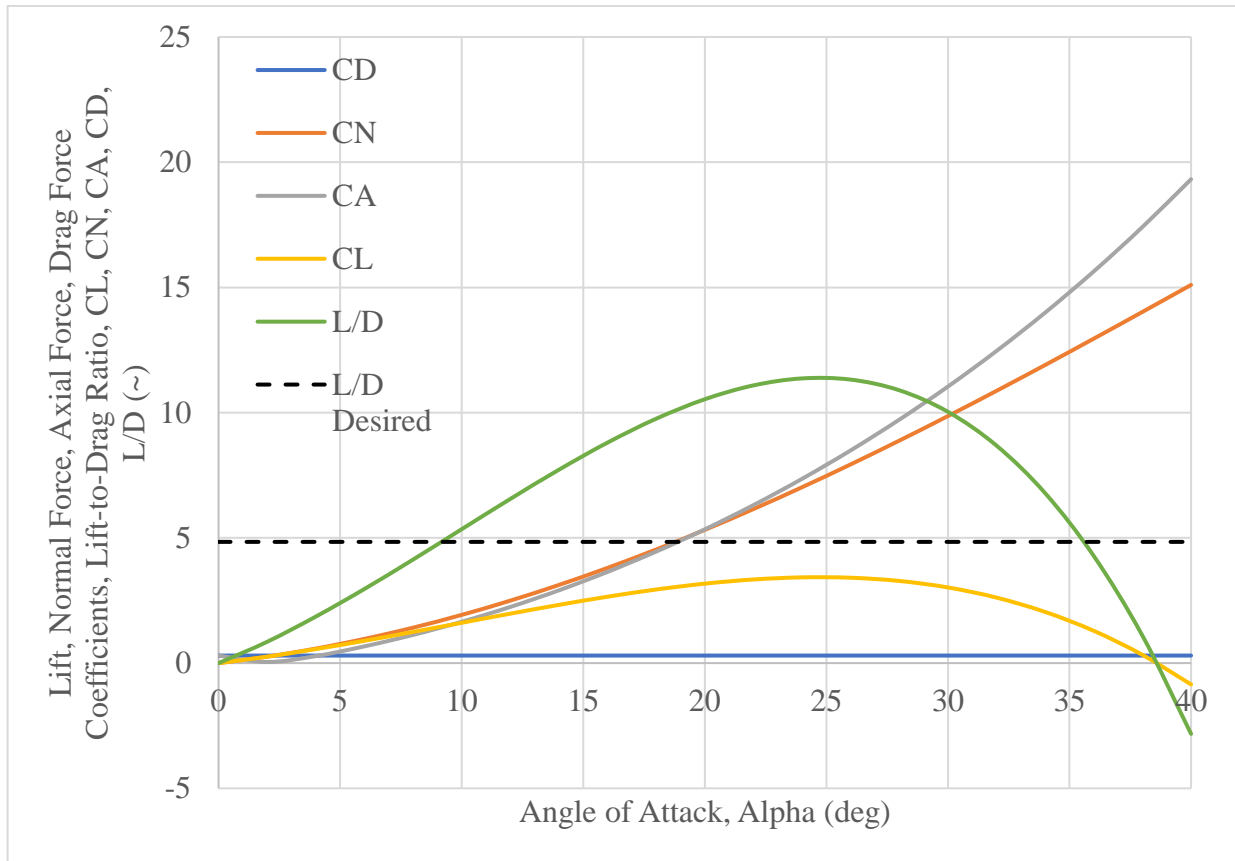


FIGURE 3-2: LIFT COEFFICIENT AT CRUISE WITH RESPECT TO ANGLE OF ATTACK

From Figure 3-2, $C_{L_{cruise}}$ is found to be [1]:

$$C_{L_{cruise}} = 1.46$$

The cruise mid-point air density (ρ_{cruise}) is found assuming a 50% fuel load. The cruise mid-point air density is defined in Equation 3.1.1 below [2]:

$$\rho_{cruise} = \frac{2(W_{Takeoff} - 0.5W_{Fuel})}{V^2 * C_{L_{cruise}} * S_{ref}} \quad (14.13.1)$$

Substituting known values obtained in previous sections, ρ_{cruise} is found to be:

$$\rho_{cruise} = \frac{2(358 \text{ lbf} - 0.5(116 \text{ lbf}))}{(3,872 \text{ ft/s})^2 * 1.46 * 0.267 \text{ ft}^2} = 1.03 \times 10^{-4} \frac{\text{lbf}}{\text{ft}^4/\text{s}^2} = 1.03 \times 10^{-4} \text{ slug/ft}^3$$

The mid-cruise point attitude is found using the cruise mid-point air density value from Section 14.13 and the Roskam Appendix to find altitude [1]. The altitude for the mid-cruise point air density at cruise is 76,000 ft. Once the AIM-120 reaches 80,000 ft at Mach 4, the RAIDER engages for terminal maneuvers.

4 RAIDER Design for Mach 4 at Burnout Altitude, Cruise Initiation Point

This section of the report details the RAIDER design for Mach 4 at burnout altitude, cruise initiation point, and the layout of the RAIDER engine.

4.1 Determination of Required Thrust at Cruise Initiation Point

The authors determine the required thrust at Cruise Initiation point for the AIM-120 missile by examining past missile design submissions. The characteristics to be obtained are the thrust required at 80,000 feet and Mach 4 flight, the cruise angle of attack (α_{cruise}), and L/D_{cruise} . Previous results are obtained at an altitude of 76,000 feet. Temperature change in this report is shown to be negligible between 45,000 feet and 76,000 feet, thus the temperature change is also considered negligible between 76,000 and 80,000 feet for this analysis. The thrust required is found in previous work to be [1]:

$$T = 70.4 \text{ lbf} \quad (4.1.1)$$

The cruise angle of attack (α_{cruise}) is found in previous work to be [1]:

$$\alpha_{cruise} = 9.2 \text{ deg} \quad (4.1.2)$$

The cruise lift versus drag ratio (L/D_{cruise}) is found in previous work to be [1]:

$$\left(\frac{L}{D}\right)_{cruise} = 4.84 \quad (4.1.3)$$

4.2 Assumptions

To proceed with calculations, the authors make the following assumptions:

- The ratio of specific heats (γ) for ramjet operation is assumed to approximately equal 1.4.
- As obtained in Section 3, the rocket motor burnout occurs at Mach 4 and 80,000 feet.
- Temperature, pressure, and area relations are obtained with isentropic relations.
- The fuel used is liquid hydrocarbon.
- The inlet is 2-D.

4.3 Calculate A_0 and A_{IT}

To calculate the inlet area (A_0), the altitude of 80,000 feet and Mach value of 4 obtained in previous sections are considered. The authors assume an initially stoichiometric fuel-air ratio (f/a). From the Fleeman text, this assumption corresponds to a (f/a) value of 0.067. The authors additionally assume a heat of combustion (H_f) value of 17,900 BTU/lbm, a freestream temperature T_0 of 390 R, and an isobaric specific heat (c_p) value of 0.302 BTU/lbm/R [3]. From previous work, the freestream pressure p_0 at 80,000 feet is found to be 58.1 psf [1]. The

nondimensional thrust equation of an ideal ramjet is given from the Fleeman text as Equation 4.3.1 [3]:

$$\frac{T}{p_0 A_0} = \gamma_0 M_0^2 \left(\left(\frac{\frac{T_4}{T_0}}{1 + \left(\frac{\gamma_0 - 1}{2}\right) M_0^2} \right)^{\frac{1}{2}} - 1 \right) \quad (4.3.1)$$

Rearranging Equation 4.3.1 for A_0 yields Equation 4.3.2:

$$A_0 = \frac{T}{p_0} \left(\gamma_0 M_0^2 \left(\left(\frac{\frac{T_4}{T_0}}{1 + \left(\frac{\gamma_0 - 1}{2}\right) M_0^2} \right)^{\frac{1}{2}} - 1 \right) \right)^{-1} \quad (4.3.2)$$

Additionally, the combustion temperature T_4 can be found using isentropic relations in Equation 4.3.3 [3]:

$$T_4 = T_0 \left(1 + \left[\left(\frac{\gamma_0 - 1}{2} \right) M_0^2 \right] \right) + \left(\frac{H_f}{c_p} \right) \left(\frac{f}{a} \right) \quad (4.3.3)$$

Substituting known values into Equation 4.3.3, T_4 is found to be:

$$T_4 = 390R \left(1 + \left[\left(\frac{1.4 - 1}{2} \right) 4^2 \right] \right) + \left(\frac{17,900}{0.302} \right) (0.067) = 5,609 R \quad (4.3.4)$$

Substituting known values into Equation 4.3.2 yields A_0 :

$$A_0 = \frac{70.4 \text{ lbf}}{58.1 \text{ psf}} \left(1.4 * 4^2 \left(\left(\frac{\frac{5,609}{390}}{1 + \left(\frac{1.4 - 1}{2}\right) 4^2} \right)^{\frac{1}{2}} - 1 \right) \right)^{-1} = 0.064 \text{ ft}^2 \quad (4.3.5)$$

Now, the mass flow of air (m_{tot}) is calculated using A_0 , m_{air} , and by assuming no spillage at the inlet area using Equation 4.3.6 [1] [4]:

$$m_{tot} = m_{air} + \left(\frac{f}{a} \right) * m_{air} \quad (4.3.6)$$

The value of m_{tot} can be found by taking the known fuel weight flow rate (W_f), assumed by the authors to be at maximum thrust, and solving for mass flow. W_f was found in previous work to be 14.85 lbf/s, and a_0 was found to be 968 ft/s [1]. The density at 80,000 ft is found to be 8.68×10^{-5} slugs/ft³ [4]. Converting to mass flow rate results in Equation 4.3.7 [4]:

$$m_{air} = \rho * (a_0 * M_0) * A_0 \quad (4.3.7)$$

Substituting in the known values, m_{air} is obtained to be:

$$m_{air} = 8.68 \times 10^{-5} \frac{\text{slug}}{\text{ft}^3} * 968 \frac{\text{ft}}{\text{s}} * 4 * 0.064 \text{ft}^2 = 0.021 \text{ slug/s} \quad (4.3.8)$$

Substituting known values, m_{tot} is found to be:

$$m_{tot} = 0.021 \frac{\text{slug}}{\text{s}} + 0.067 * 0.021 \frac{\text{slug}}{\text{s}} = 0.023 \text{ slug/s} \quad (4.3.9)$$

Now, the authors assume the inlet start Mach number (M_{IE}) begins at Mach 1.5 and that the inlet is a quasi-isentropic compression spike to find the inlet throat area (A_{IT}) using Equation 4.3.10 [3]:

$$\frac{A_{IT}}{A_0} = 1.728 * (M_{IE})_{start} [1 + 0.2(M_{IE})^2_{start}]^{-3} \quad (4.3.10)$$

Solving Equation for A_{IT} yields Equation 4.3.11:

$$A_{IT} = 1.728 * A_0 * (M_{IE})_{start} [1 + 0.2(M_{IE})^2_{start}]^{-3} \quad (4.3.11)$$

Substituting in known values, the A_{IT} is found to be:

$$A_{IT} = 1.728 * 0.064 \text{ft}^2 * 1.5 [1 + 0.2 * 1.5^2]^{-3} = 0.054 \text{ft}^2 \quad (4.3.12)$$

4.4 Combustor Inlet Mach Number and Area, Exit Mach Number, and Pressure

To calculate the combustor inlet Mach number M_3 and area A_3 , exit Mach number M_4 , and pressure p_4 , the Fleeman text is utilized. To find M_3 , the combustor to freestream temperature ratio T_4/T_0 is utilized. T_4/T_0 is found to be:

$$\frac{T_4}{T_0} = \frac{5,609 \text{ R}}{390 \text{ R}} = 14.4 \quad (4.4.1)$$

From the Fleeman text, a ratio like T_4/T_0 for a given value of the total combustor to freestream temperature ratio (T_{4t}/T_0) is used, which the authors assume to be 15. Using Figure 3.30 from the Fleeman text, and conservatively assuming a Mach that causes thermal choking, M_3 is estimated to be [3]:

$$M_3 = 0.23$$

Using M_3 , A_3 is found from the Fleeman text using Equation 4.4.2 [3]:

$$\frac{A_{IT}}{A_3} = \left(\frac{1.728 * M_3}{(1 + (0.2 * M_3^2))^3} \right) \quad (4.4.2)$$

Rearranging Equation 4.4.2 for A_3 yields:

$$A_3 = A_{IT} \left(\frac{1.728 * M_3}{(1 + (0.2 * M_3^2))^3} \right)^{-1} \quad (4.4.3)$$

Substituting in known values, A_3 is found to be:

$$A_3 = 0.054 ft^2 \left(\frac{1.728 * 0.23}{(1 + (0.2 * 0.23^2))^3} \right)^{-1} = 0.14 ft^2 \quad (4.4.4)$$

To find M_4 , T_3 must first be found using Equation 4.4.5 [3]:

$$T_3 = T_0[1 + 0.2 * M_0^2] \quad (4.4.5)$$

Substituting known values, T_3 is found to be:

$$T_3 \sim T_{3t} = 390R * [1 + 0.2 * 4^2] = 1,640 R \quad (4.4.6)$$

Now, Equation 4.4.7 from the Fleeman text is utilized to solve for M_4 [3]:

$$\frac{T_{4t}}{T_{3t}} = \left(\frac{M_4}{M_3} \right)^2 \left\{ 1 + \left(\frac{\left[\frac{\gamma - 1}{2} \right] * M_4^2}{[1 + * \gamma M_4^2]^2} \right) \right\} \quad (4.4.7)$$

The authors assume a standard γ value for the hydrocarbon fuel to be 1.35 [3]. This equation is rearranged into quadratic form in the Fleeman text to solve for M_4 , and is composed of Equations 4.4.8 through 4.4.11 [3]:

$$M_4 \cong \left\{ \frac{[-b - (b^2 - 4ac)^{1/2}]}{2a} \right\}^{1/2} \quad (4.4.8)$$

The terms “a,” “b,” and “c” are outlined as [3]:

$$a = 1.822 \left(\frac{T_{4t}}{T_{3t}} \right) M_3^2 - 1.175 \quad (4.4.9)$$

$$b = 2.70 \left(\frac{T_{4t}}{T_{3t}} \right) M_3^2 \quad (4.4.10)$$

$$c = \left(\frac{T_{4t}}{T_{3t}} \right) M_3^2 \quad (4.4.11)$$

Substituting known values into Equations 4.4.4-11 yields the term values:

$$a = 1.822 \left(\frac{5,609 R}{1,640 R} \right) 0.23^2 - 1.175 = -0.845 \quad (4.4.12)$$

$$b = 2.70 \left(\frac{5,609 R}{1,640 R} \right) 0.23^2 = 0.488 \quad (4.4.13)$$

$$c = \left(\frac{5,609 R}{1,640 R} \right) 0.23^2 = 0.181 \quad (4.4.14)$$

Substituting the terms back into Equation 4.4.8 yields M_4 :

$$M_4 \cong \left\{ \frac{\left[-(0.488) - \left((0.488)^2 - 4(-0.845)(0.181) \right)^{\frac{1}{2}} \right]}{2(-0.845)} \right\}^{\frac{1}{2}} = 0.91 \quad (4.4.15)$$

To find p_4 , isentropic inlet conditions are assumed. The total freestream pressure p_{t0} is calculated using isentropic relations to be [4]:

$$p_{t0} = p_0 \left(1 + \frac{\gamma_0 - 1}{2} M_0^2 \right)^{\frac{\gamma_0}{\gamma_0 - 1}} \quad (4.4.16)$$

Substituting known values, p_{t0} is found to be:

$$p_{t0} = 58.1 \text{ psf} \left(1 + \frac{1.4 - 1}{2} (4^2) \right)^{\frac{1.4}{1.4 - 1}} = 8,820 \text{ psf} \quad (4.4.17)$$

Now, the authors assume no loss in total pressure throughout the intake [3]:

$$p_{t3} = p_{t0} \quad (4.4.18)$$

Using this relation and M_3 , p_3 can be found through isentropic relations and an assumed γ_3 value of 1.35 to be [3] :

$$p_3 = 8,820 \text{ psf} \left(1 + \frac{1.35 - 1}{2} (0.23^2) \right)^{\frac{-1.35}{1.35 - 1}} = 8,510 \text{ psf} \quad (4.4.19)$$

From the Fleeman text, for M_3 of 0.23, the ratio of the p_4/p_3 is found to be 0.85 [3]. Therefore, p_4 is found to be:

$$p_4 = 0.85 * (8,510 \text{ psf}) = 7,240 \text{ psf} \quad (4.4.20)$$

The authors realize that isentropic and zero total pressure loss assumptions may yield inaccurate results, and further survey in literature outside of the Fleeman text is needed for ramjet analysis to obtain higher fidelity methods and results [3]. Finally, the total pressure loss between the combustor inlet and combustion chamber can be found using Equation 4.4.21 from the Fleeman text [3]:

$$\frac{p_{4t}}{p_{3t}} = \frac{\left\{ 1 + \left[\frac{\gamma - 1}{2} \right] M_4^2 \right\}^{\frac{\gamma}{\gamma - 1}}}{1 + \gamma M_4^2} \quad (4.4.21)$$

Substituting known values, the pressure loss is found to be:

$$\frac{p_{4t}}{p_{3t}} = \frac{\left\{ 1 + \left[\frac{1.35 - 1}{2} \right] 0.91^2 \right\}^{\frac{1.35}{1.35 - 1}}}{1 + 1.35 * 0.91^2} = 0.80 \quad (4.4.22)$$

4.5 Speed of Sound in Combustion Chamber

The authors calculated the speed of sound in the combustion chamber, a_4 , by using T_4 and an estimate for the ratio of specific heats, γ . The equation used to calculate the speed of sound is presented in Equation 4.5.1 below as [4]:

$$a_4 = \sqrt{\gamma RT_4} \quad (4.5.1)$$

In this equation, R is the gas constant and is equal to 1,716 ft-lbf/slug-R. Substituting the known value for T_4 , the estimated ratio of specific heats, and the gas constant R , a_4 is found to be:

$$a_4 = \sqrt{1.4 * 1716 * 5,609} = 3,670 \text{ ft/s} \quad (4.5.2)$$

4.6 Combustion Speed, V_4

The combustion speed, V_4 , is determined using previously obtained M_4 and a_4 values. The combustion speed is found using Equation 4.6.1 below [4]:

$$V_4 = a_4 * M_4 \quad (4.6.1)$$

Substituting in the known values, V_4 is found to be:

$$V_4 = 3,670 \frac{\text{ft}}{\text{s}} * 0.91 = 3,340 \text{ ft/s} \quad (4.6.2)$$

4.7 Combustion Chamber Length Calculation, L_c

The combustion chamber length L_c is found using the combustion speed V_4 obtained previously and assuming typical combustion times as found in the text [3]. The typical combustion time t_{comb} for a supersonic combustion ramjet is determined to be 0.002 s [3]. The length of the combustion chamber is calculated using Equation 4.7.1 [3]:

$$L_c = t_{\text{comb}} * V_4 \quad (4.7.1)$$

Substituting in known values, the minimum combustion chamber length is found to be:

$$L_c = 0.002\text{s} * 3,340 \text{ ft/s} = 6.7 \text{ ft} \quad (4.7.2)$$

The assumption of a 0.002 s combustion time is rather conservative, and therefore leads to an excessively long minimum L_c . When the authors abandon this assumption and assume very ideal combustion conditions (0.001 s), L_c becomes:

$$L_c = 0.001\text{s} * 3,340 \text{ ft/s} = 3.3 \text{ ft} \quad (4.7.3)$$

Assuming very ideal combustion conditions allows the L_c to account for slightly less than half the missile length of 7.5 ft.

4.8 Throat Area Determination

To determine the throat area for sonic choking, the authors assume a characteristic velocity (c^*) at a nominal value of 5,200 ft/s and the acceleration due to gravity (g) to be 32.2 ft/s². The total mass flow rate, m_{tot} , is obtained from previous work [1]. In this estimation, p_4 is assumed to be the combustion chamber pressure:

$$p_c = p_4 \quad (4.8.1)$$

Utilizing Figure 3.53 in the Fleeman text, assuming the chamber pressure is slightly above the Fleeman value at 2,000 psf, the throat area A_t is found using Equation 4.8.2 [3]:

$$W_f = \frac{g * p_c * A_t}{c^*} \quad (4.8.2)$$

Rearranging to solve for A_t and substituting known values where W_f is a substitute for the total mass flow rate m_{tot} , A_t is found to be [1]:

$$A_t = \frac{5,200 \frac{ft}{s} * 0.023 \frac{slug}{s} * 32.2 \frac{lb}{slug}}{32.2 \frac{ft}{s^2} * 7,240 \text{ psf}} = 0.018 \text{ ft}^2 \quad (4.8.3)$$

4.9 Expansion Bell/ Nozzle Design

To design the expansion bell for the AIM-120 missile, the authors assume that the expansion bell is configured by multiplying 1.1 to the projectile diameter to find the expansion bell/nozzle. Equation 4.9.1 shows the calculation to find the expansion bell/nozzle diameter. The equation found that the expansion bell/nozzle diameter is 5.01 inches. This means that there should be a flare look to the aft portion of the missile due to the size increase between the missile diameter and the expansion bell/nozzle.

$$\text{Nozzle Diameter} = 1.1 * 4.55 \text{ in} = 5.01 \text{ in} \quad (4.9.1)$$

Due to the nozzle diameter increase there is an addition of a ‘flare’ to the end to allow for the correct sizing of the expansion bell/nozzle. Figure 4-1 shows a model of what the expansion bell should look like on the missile.

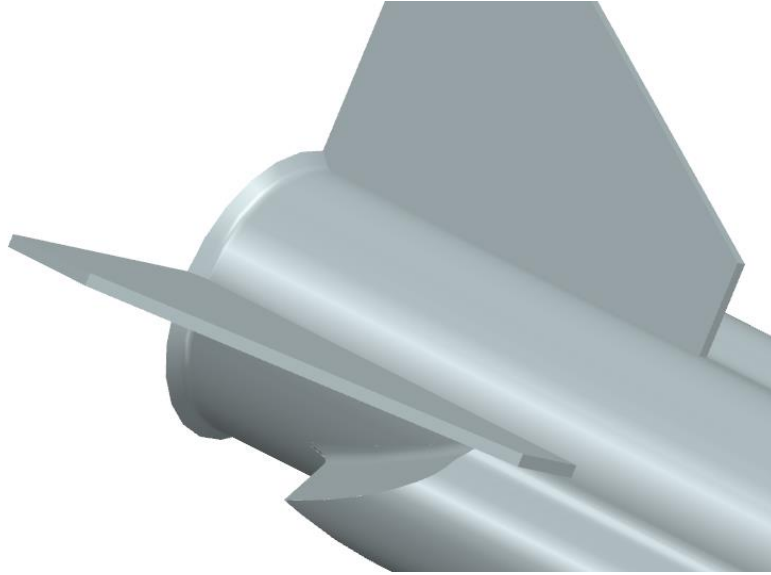


FIGURE 4-1: AIM-120 RAIDER EXPANSION BELL/NOZZLE ADDITION

4.10 Engine Thrust and I_{sp}

To determine the engine thrust (T) and specific impulse (I_{sp}) of the missile given the estimations made in this report section and new design considerations, techniques in Fleeman were utilized. The equations for specific impulse and thrust are shown below as Equations 4.10.1 and 4.10.2, assuming isentropic flow [3]:

$$I = c_d \left\{ \left(\left[\frac{2\gamma^2}{\gamma-1} \right] \left[\frac{2}{\gamma+1} \right]^{\frac{\gamma+1}{\gamma-1}} \left[1 - \frac{p_e}{p_c} \right] \right)^{\frac{1}{2}} + \left(\frac{p_e}{p_c} \right) \varepsilon - \left(\frac{p_0}{p_c} \right) \varepsilon \right\} * \frac{c^*}{g} \quad (4.10.1)$$

$$T = \left(\frac{g}{c^*} \right) p_c * A_t * I_{sp} \quad (4.10.2)$$

In these equations, c_d is the discharge efficiency coefficient and assumed to be 0.96, γ is assumed to be 1.18, c^* is assumed to be a nominal 5,200 ft/s, p_e is the exit pressure, p_0 is the freestream pressure, and p_c is the chamber pressure from Section 4.8 [3]. The nozzle expansion ratio, ε , is found using Equation 4.10.3 [3]:

$$\varepsilon = \frac{\left\{ \left[\frac{2}{\gamma+1} \right]^{\frac{1}{\gamma-1}} \left[\frac{\gamma-1}{\gamma+1} \right]^{\frac{1}{2}} \right\}}{\left\{ \left(\frac{p_e}{p_c} \right)^{\frac{1}{\gamma}} * \left[1 - \left(\frac{p_e}{p_c} \right)^{\frac{\gamma-1}{\gamma}} \right]^{1/2} \right\}} \quad (4.10.3)$$

Additionally, the ratio between exit pressure and chamber pressure is assumed to be approximately 0.025 from the Fleeman text [3]. The value of p_e is then found to be:

$$p_e = 7,240 \text{ psf} * 0.025 \cong 180 \text{ psf} \quad (4.10.3)$$

Substituting known values, ε is found to be:

$$\varepsilon = \frac{\left\{ \left[\frac{2}{1.18 + 1} \right]^{\frac{1}{1.18-1}} \left[\frac{1.18 - 1}{1.18 + 1} \right]^{\frac{1}{2}} \right\}}{\left\{ \left(\frac{180}{7,240} \right)^{\frac{1}{1.18}} * \left[1 - \left(\frac{180}{7,240} \right)^{\frac{1.18-1}{1.18}} \right]^{1/2} \right\}} = 6.2 \quad (4.10.4)$$

Now, ε is substituted into Equation 4.10.1 to find I_{sp} :

$$I_{sp} = 0.96 \left\{ \left\{ \left[\frac{2(1.18)^2}{1.18 - 1} \right] \left[\frac{2}{1.18 + 1} \right]^{\frac{1.18+1}{1.18-1}} \left[1 - \frac{180}{7,240} \right] \right\}^{\frac{1}{2}} + \left(\frac{180}{7,240} \right) 6.2 - \left(\frac{58.1}{7,240} \right) 6.2 \right\} * \frac{5,200 \text{ ft/s}}{32.2 \text{ ft/s}^2} \cong 374 \text{ s} \quad (4.10.5)$$

Finally, the thrust can be obtained as:

$$T = \left(\frac{32.2 \text{ ft/s}^2}{5,200 \text{ ft/s}} \right) * 7,240 \text{ psf} * 0.033 \text{ ft}^2 * 374 \text{ s} = 553 \text{ lbf} \quad (4.10.6)$$

5 Design Iteration and Optimization

This section of the report details the design iteration and optimization of the AIM-120 RAIDER. Figure 5-1 shows a preliminary representation of what the redesigned AIM-120 RAIDER missile interior should look like from the results of Sections 2, 3, 4, and previous work [1]. The grey colored areas show the skin or the components section of the missile while the black/dark grey sections show the internal airducts and the combustion chamber.

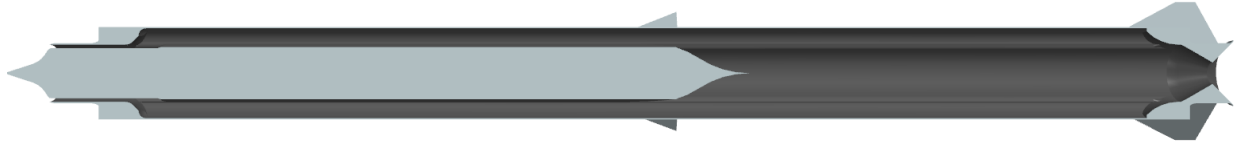


FIGURE 5-1: AIM-120 RAIDER COMBUSTION CONFIGURATION SETUP

The authors performed five iterations upon the preliminary RAIDER configuration to converge upon a final redesign which, with development, would be workable and feasible. The authors focused on decreasing the area of the inlet to increase aerodynamic performance, while maintaining thrust at above an altitude of 65,000 feet.

5.1 Iteration Process

The first step in the iteration of the propulsion system is determining a new inlet area. The inlet area found in section 4.3 was multiplied by a percentage of decrease, seen as d_i in Equation 5.1.1 to find the new inlet area.

$$A_{0_i} = A_0 d_i \quad (5.1.1)$$

Equation 4.3.1 was rearranged to solve for p_0 while maintaining performance with the decreased inlet area. The new inlet area was then plugged into Equation 5.1.2 while keeping all other values the same as in section 4.

$$p_0 = \frac{T}{A_0} \left(\gamma_0 M_0^2 \left(\left(\frac{\frac{T_4}{T_0}}{1 + \left(\frac{\gamma_0 - 1}{2} \right) M_0^2} \right)^{\frac{1}{2}} - 1 \right) \right)^{-1} \quad (5.1.2)$$

The freestream pressure calculated was then cross-referenced with the appendix in John Anderson's textbook to find the altitude the missile would have to fly at to achieve that pressure. The density of air at that altitude was then used to find the mass flow rate of air the missile would ingest. The rest of the calculations were completed in the same manner as section 4. The altitude, inlet throat diameter, throat diameter, and thrust available from the engine with the new inlet area were analyzed to determine whether the new inlet area was an improvement or not.

5.2 Iteration 1

The inlet area was first decreased to 95% of the original size. The resulting missile parameters can be seen below in Table 5-1.

TABLE 5-1: ITERATION 1 MISSILE PARAMETERS

Altitude	79,000 ft
Inlet Diameter	3.33 in
Inlet Throat Diameter	3.07 in
Throat Diameter	1.74 in
Thrust	273 lb

The cruise altitude to achieve similar performance was decreased slightly, while well above the minimum altitude. The thrust also remained similar as in section 4, well above what the missile requires for cruise. All diameters decreased.

5.3 Iteration 2

Due to the minimal decrease in cruise altitude, the inlet area was decreased significantly more by 80%. The missile parameters from this inlet area are seen below in Table 5-2.

TABLE 5-2: ITERATION 2 MISSILE PARAMETERS

Altitude	75,500 ft
Inlet Diameter	3.05 in
Inlet Throat Diameter	2.82 in
Throat Diameter	1.60 in
Thrust	272 lb

The altitude and thrust are still satisfactory for the missile, while the diameters decreased. The inlet area could be further decreased.

5.4 Iteration 3

The third iteration was a 70% decrease in the initial inlet area. The parameters calculated from this decrease can be found below in Table 5-3.

TABLE 5-3: ITERATION 3 MISSILE PARAMETERS

Altitude	72,500 ft
Inlet Diameter	2.86 in
Inlet Throat Diameter	2.63 in
Throat Diameter	1.50 in
Thrust	274 lb

The altitude and thrust are still satisfactory for the missile, although the thrust is greater than the 80% inlet area model. All diameters of the propulsion system decreased further. The inlet area could be further decreased.

5.5 Iteration 4

The inlet area was brought down to 60% of the original size, which resulted in the parameters listed in Table 5-4.

TABLE 5-4: ITERATION 4 MISSILE PARAMETERS

Altitude	69,500 ft
Inlet Diameter	2.65 in
Inlet Throat Diameter	2.44 in
Throat Diameter	1.38 in
Thrust	271 lb

The altitude the missile must cruise at with this size of inlet area is close to the minimum altitude, but a further decrease is available. The thrust is still adequate, a slight decrease, and the diameters have decreased.

5.6 Iteration 5

The final iteration of the missile was a 50% size inlet area, which resulted in the parameters listed in Table 5-5.

TABLE 5-5: ITERATION 5 MISSILE PARAMETERS

Altitude	65,500 ft
Inlet Diameter	2.41 in
Inlet Throat Diameter	2.23 in
Throat Diameter	1.27 in
Thrust	274 lb

The cruise altitude is just above the minimum altitude of 65,000 feet, which means the inlet area should not be decreased further. The thrust available is maintained, meaning the missile will keep the same performance. The diameters throughout the propulsion system have been decreased significantly, which allows the aerodynamic qualities of the missile to be improved. Section 6 includes models of each iteration of the missile.

5.7 Materials

The following materials were researched for optimizing the structure of the inflatable ducts, including some that are “unusual” for aerospace applications. Finally, the most feasible material for manufacturing was to be chosen.

First, piezoelectric materials were initially considered for the inflatable ducts, but the high levels of stress a missile undergoes in-flight would make these unsuitable for the application.

Secondly, certain grades of steel were looked at for the application. Maraging steels were considered for their superior strength and toughness under high pressures, but they'd be too difficult to weld into the missile body.

Next, Inconel-X, a precipitation hardenable nickel-chromium alloy was looked at for the ducts due to their high strength under high temperatures, excellent workability in terms of machining and welding, a high resistance to corrosion in both oxidizing and reducing conditions as well as stress corrosion cracking. This would be a great fit for the ducts as the material properties are desirable and it can be easily welded on. Additionally, the corrosion resistance would help it stay mission ready while in storage.

Finally, shape memory alloys were researched as potential materials for building inflatable ducts due to their unique structural ability. Nitinol was considered for a variety of reasons including its light weight, the ability to “memorize” a particular geometry, high tensile strength, high melting point and great corrosion resistance. However, welding it is very difficult and the process may deteriorate its mechanical properties. Additionally, it is expensive to acquire.

In terms of manufacturability, Inconel-X is the best metal of those researched to build the inflatable tubes for the AIM-120 AMRAAM RAIDER. It is the only material machinable enough to weld the tubes onto the missile. Inconel-X is also an attractive metal from a cost perspective as it is the cheapest metal strong enough for the application. However, it is the densest metal that the authors have researched, making it the heaviest metal for the application. This is a big downside, as one of aims of the optimization process is to reduce the weight of missile to maintain its range.

Further research was conducted into other regular aerospace grade metals to provide a good mix of structural strength combined with low cost and light weight. The properties of titanium were researched, and it proved to be an attractive metal to use on the missile as it was lightest and least expensive while still being strong enough in tension to compare to the other alloys researched. Additionally, most of the body of the AIM-120 AMRAAM is made of titanium so making the inflatable tubes out of titanium would aid manufacturability and stop galvanic corrosion. Thus, according to the authors, titanium would be the best choice of metal to use for making the inflatable ducts.

Table 5-6 below displays the base cost of each material and the associated weight of material needed to make each of the inflatable ducts.

TABLE 5-6: INFLATABLE DUCT MATERIALS [5] [6] [7] [8] [9] [10] [11] [12]

Material	Density (lb/in³)	Cost (\$/lb)	Weight of ducts (lb)	Cost of ducts (\$)
Maraging steel	0.289	43	4.49	193
Inconel - X	0.299	46	4.64	213
Nitinol	0.233	18.14	3.62	65.6
Titanium	0.163	30	2.53	75.9

6 Final RAIDER Weapon CAD Figures

This section of the report details the final AIM-120 RAIDER weapon design CAD figures. Three variants of the weapon system are created in CAD software, and each is displayed in four-view, full-color cutaway, stowed, separated, and dash/ terminal configurations.

6.1 Four-View

The four-view CAD configurations of the missile along with the nose diameter are displayed in Figures 6-1 through 6-6 below.

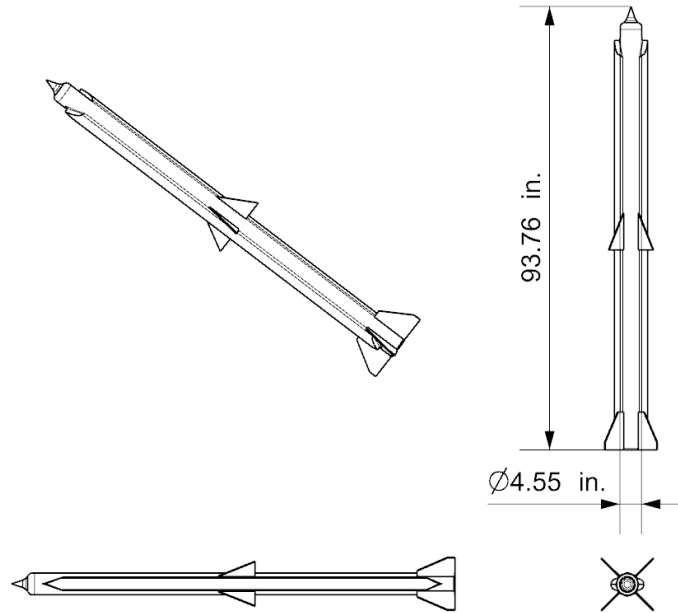


FIGURE 6-1: ITERATION 1 FOUR-VIEW

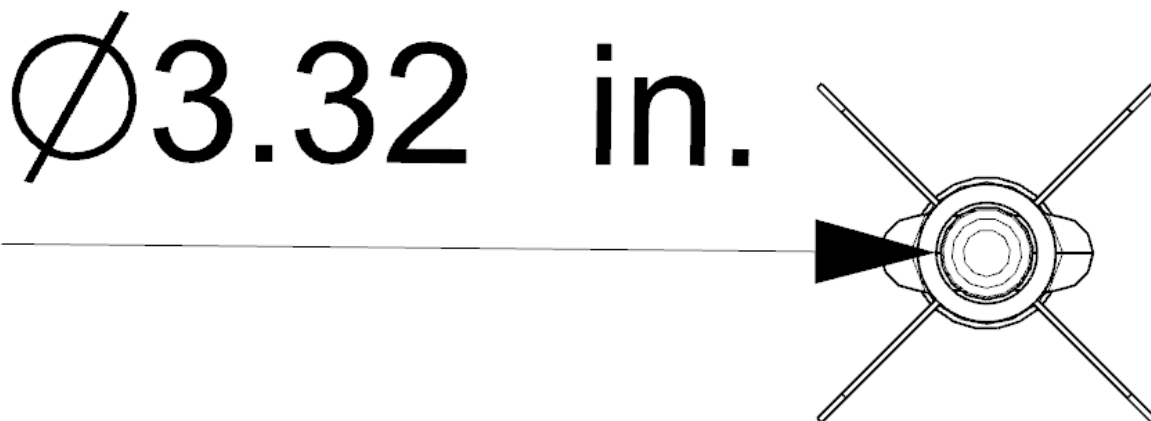


FIGURE 6-2: ITERATION 1 NOSE DIAMETER

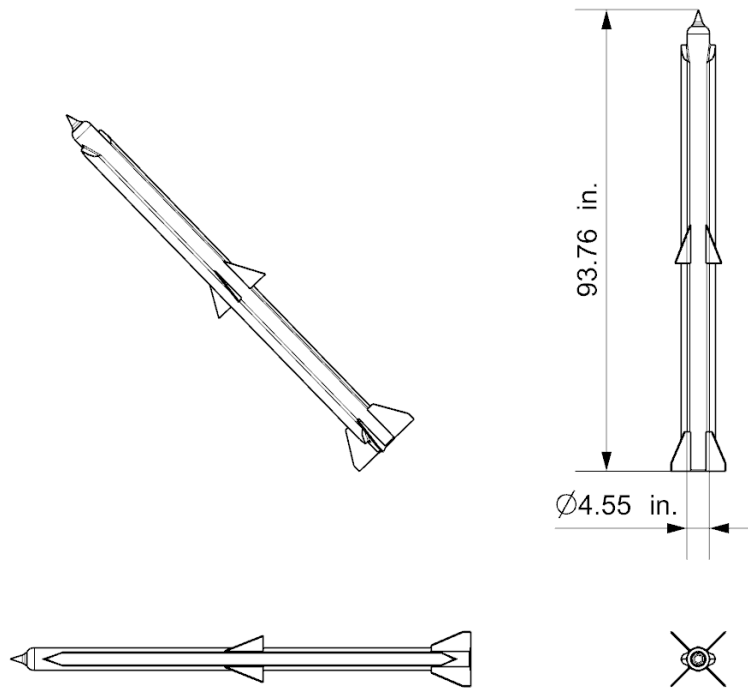


FIGURE 6-3: ITERATION 2 FOUR-VIEW

$\text{Ø}3.05$ in.

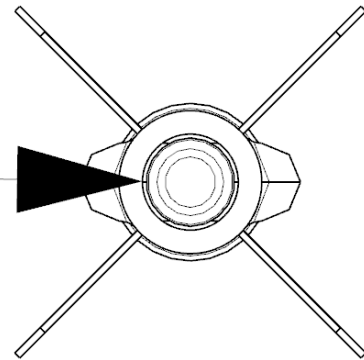


FIGURE 6-4: ITERATION 2 NOSE DIAMETER

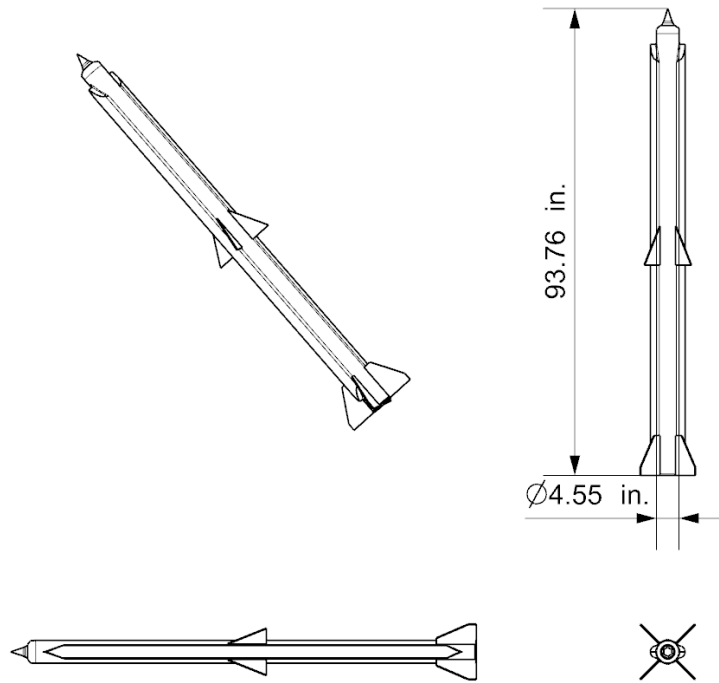


FIGURE 6-5: ITERATION 3 FOUR-VIEW

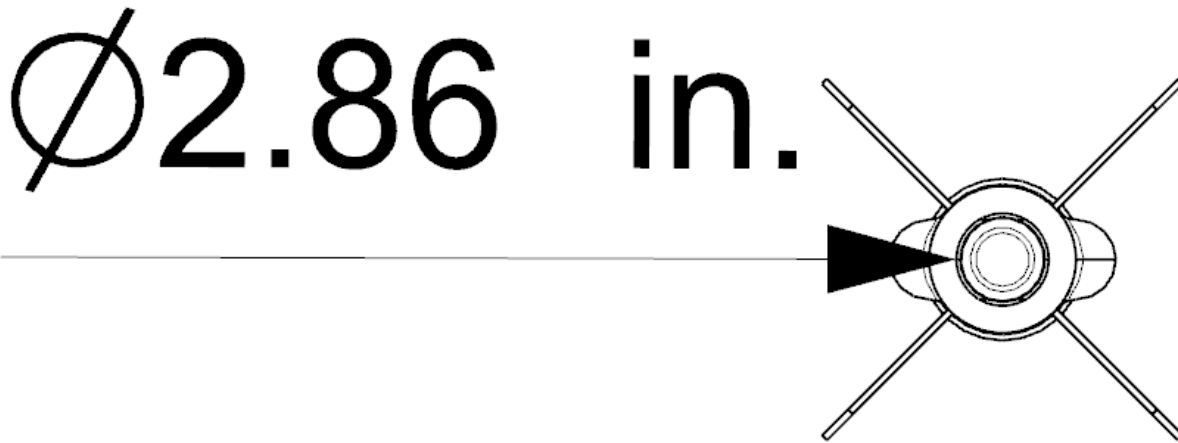


FIGURE 6-6: ITERATION 3 NOSE DIAMETER

6.2 Full-Color Cutaway

The full-color cutaway CAD configurations of the missile are displayed in Figures 6-7 through 6-9 below.

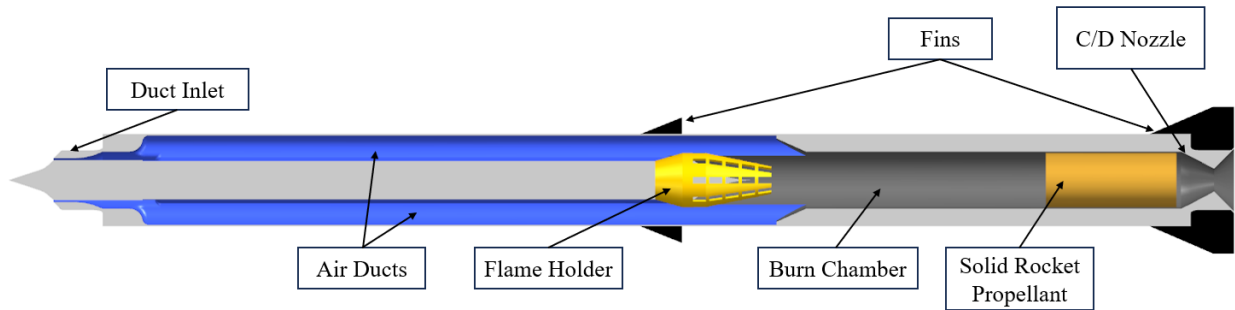


FIGURE 6-7: ITERATION 1 FULL-COLOR CUTAWAY

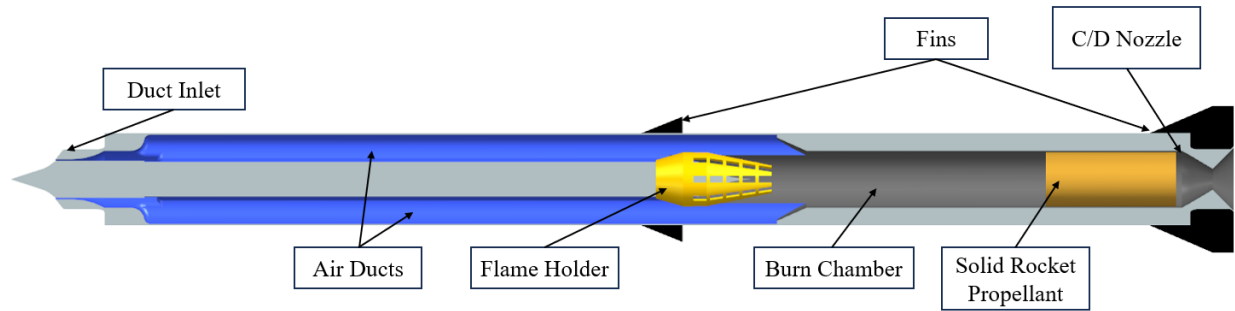


FIGURE 6-8: ITERATION 2 FULL-COLOR CUTAWAY

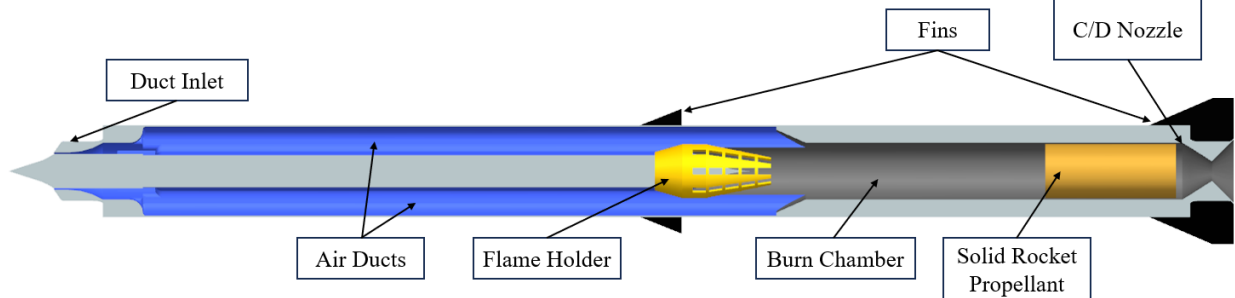


FIGURE 6-9: ITERATION 3 FULL-COLOR CUTAWAY

6.3 Fully Collapsed/ Stowed

The fully collapsed/ stowed variant CAD configurations of the missile are displayed in Figures 6-7 through 6-9 below.

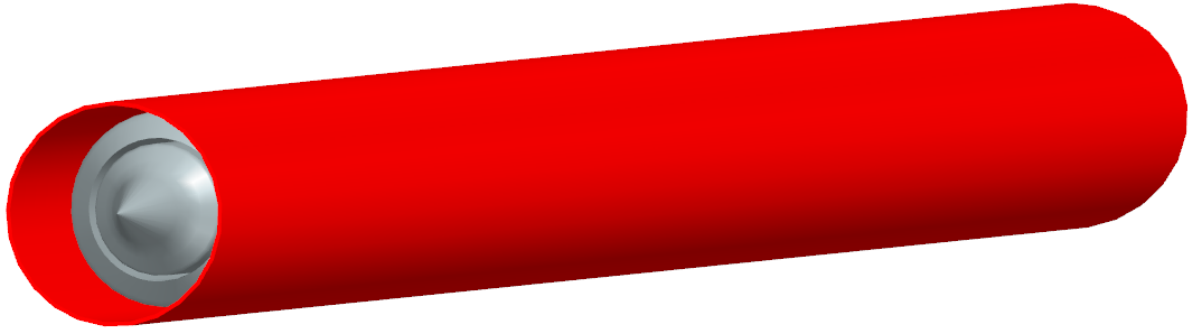


FIGURE 6-10: ITERATION 1 FULLY COLLAPSED/ STOWED

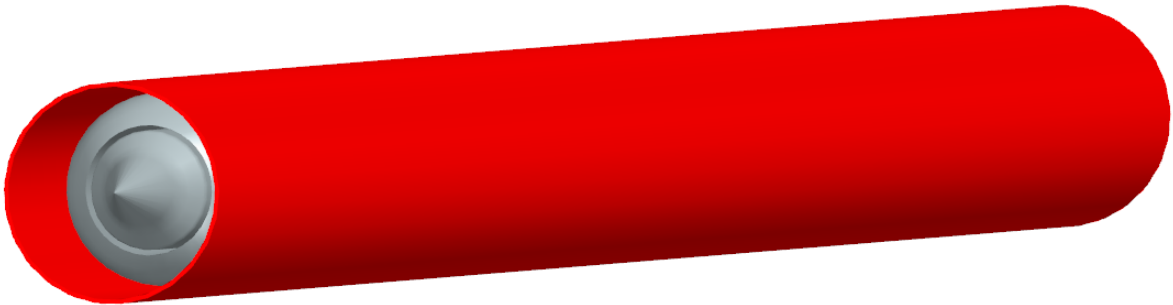


FIGURE 6-11: ITERATION 2 FULLY COLLAPSED/ STOWED

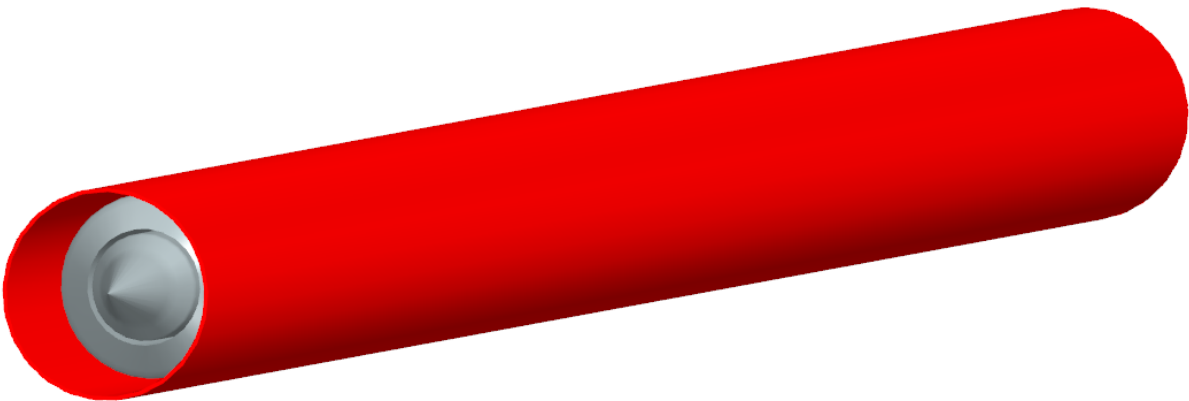


FIGURE 6-12: ITERATION 3 FULLY COLLAPSED/ STOWED

6.4 Separated

The authors define the “separated” configuration to be just post-launch, where all ducts and control surfaces are in stowed positions and the boosting rocket motor burns out. The separated variant CAD configurations are displayed in Figures 6-10 through 6-12 below.

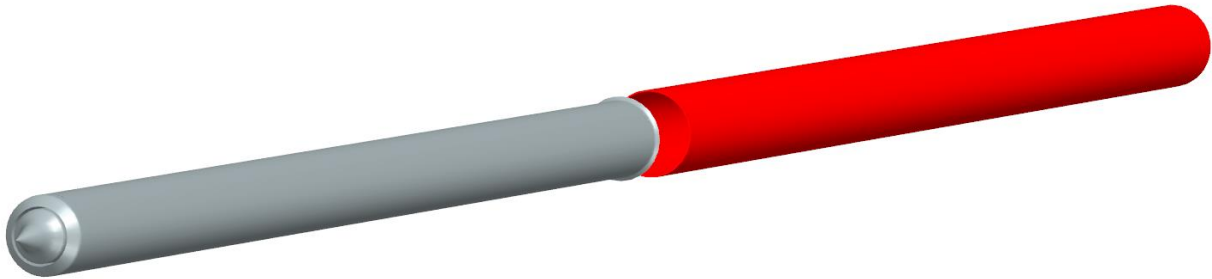


FIGURE 6-13: ITERATION 1 SEPARATED

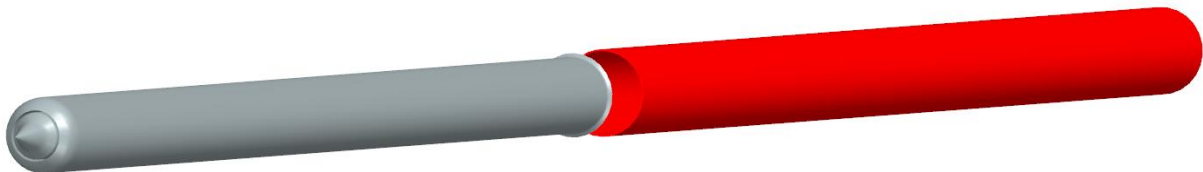


FIGURE 6-14: ITERATION 2 SEPARATED

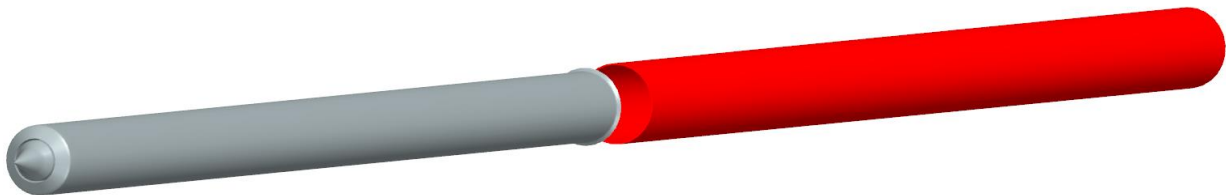


FIGURE 6-15: ITERATION 3 SEPARATED

6.5 Dash and Terminal Configuration

In the dash and terminal configuration, the weapon system features all systems in a deployed configuration. The dash and terminal variant CAD configurations are displayed in Figures 6-13 through 6-15 below.

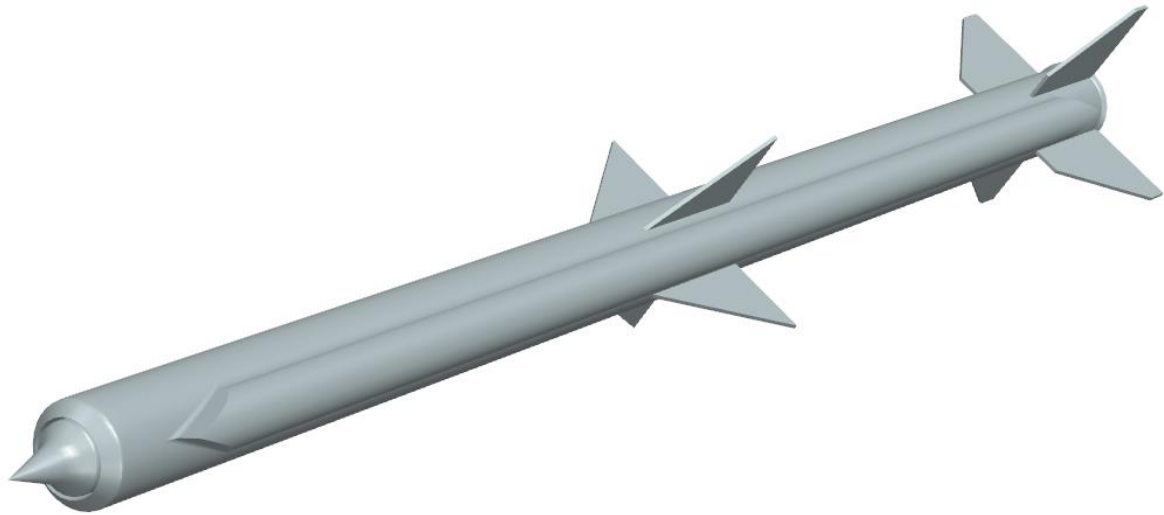


FIGURE 6-16: ITERATION 1 DASH AND TERMINAL

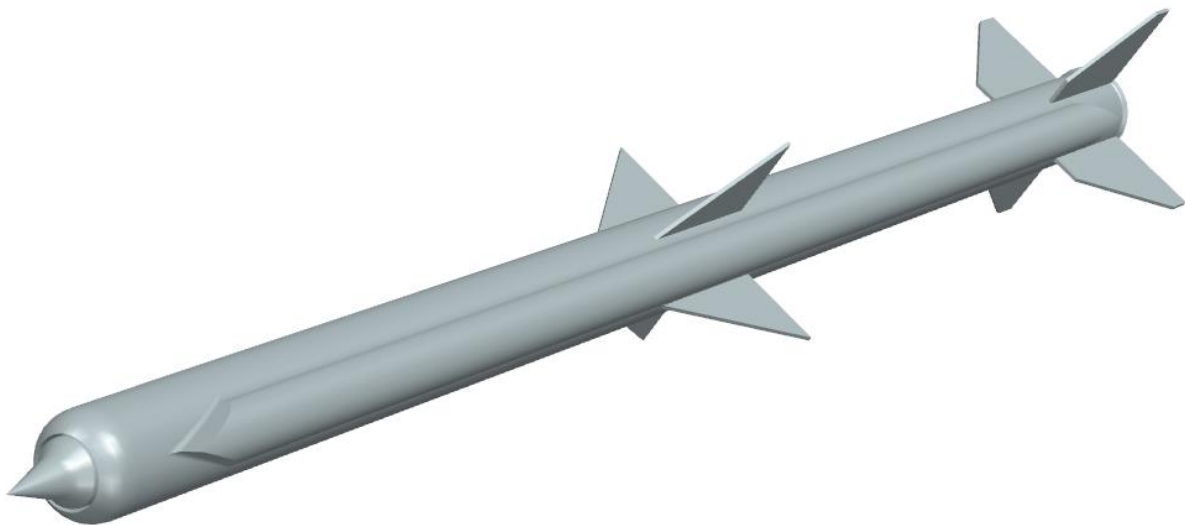


FIGURE 6-17: ITERATION 2 DASH AND TERMINAL

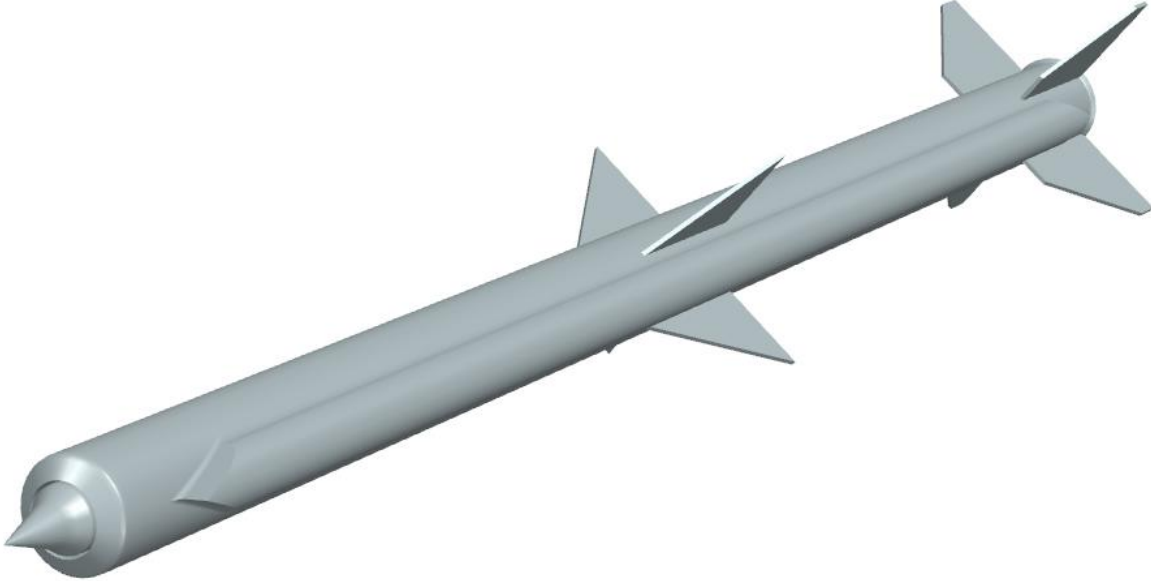


FIGURE 6-18: ITERATION 3 DASH AND TERMINAL

7 Conclusions and Recommendations

7.1 Conclusions

- The AIM-120D-3 is the benchmark missile configuration chosen by the authors to be improved upon.
- Missile drag increase is marginal between Mach 1 and 2 between 50-150 lbf, and significant between Mach 2 and 3 (particularly at low altitude) with an approximately 1000lbf difference.
- The use of high-strength aluminum increases the E_t/W of the missile and thus its first bending frequency at which the structure deflects.
- Missile L/D is highest at approximately a 12-degree angle of attack – optimum performance is reached with low drag characteristics and a high fineness ratio.
- L/D with respect to angle of attack and Mach number increases with altitude and decreases as each parameter increases.
- The volumetric efficiency of 3.22 and L/D of 0.0905 indicate a high radar cross-section.
- The highest backward A.C. shift rate occurs between Mach 1.25 and 2.5, with the greatest differential of increase rate in backward A.C. shift between an A of 1 and 2.
- The missile body A.C. location shift with respect to α with the addition of a flare is greater than without a flare.
- The hinge moments are negative for both the wings and tail because the Aspect Ratios of the AIM-120 planar surfaces are small.
- The length of the combustion chamber is 3.3 feet.
- The optimized thrust produced is 553 lbf and the optimized I_{SP} of the missile is 374 seconds.
- The optimized inlet diameter is 2.86 inches and the optimized nozzle throat diameter is 1.5 inches.
- The inflatable ducts should be made out of military grade titanium to reduce overall cost and weight of the missile.

Additionally, salient and performance characteristics of prior AIM-120 variants are compiled and displayed in Table 5-1 and 5-2 below, respectively. Performance characteristics beyond range cannot be obtained with high fidelity, and thus benchmarking could be improved by author clearance to classified performance data.

TABLE 10-17-1: GEOMETRIC AND SALIENT CHARACTERISTICS OF PRIOR VARIANTS [3]

<i>Quality</i>	AIM 120 A	AIM 120 B	AIM 120 C3	AIM 120 C4	AIM 120 C5	AIM 120 C6	AIM 120 C7
<i>Diameter (m)</i>	1.78	1.78	1.78	1.78	1.78	1.78	1.78
<i>Length (m)</i>	3.65	3.65	3.65	3.65	3.65	3.65	3.65
<i>Launch Weight (kg)</i>	157.8	157.8	157.8	157.8	161.5	161.5	161.5
<i>Warhead (kg)</i>	22 kg HE blast fragmentation	22 kg HE	20 kg HE	20 kg HE	20 kg HE	20 kg HE	20 kg HE
<i>Wingspan (m)</i>	0.53	0.53	0.484	0.484	0.484	0.484	0.484

TABLE 10-27-2: PERFORMANCE DATA OF PRIOR VARIANTS [15]

<i>Quality</i>	AIM 120 A	AIM 120 B	AIM 120 C3	AIM 120 C4	AIM 120 C5	AIM 120 C6	AIM 120 C7
<i>Range (km)</i>	50-70	50-70	50-70	50-70	>105	>105	120

7.2 Recommendations

This section details the recommendations for the AIM-120 benchmark outlined in this report. The authors recommend that higher fidelity codes be used to benchmark the missile, and that Computational Fluid Dynamics be used to accurately ascertain the aerodynamic capabilities of the benchmark missile. The authors further recommend:

- The drag increase above Mach 2 can be remedied with drag-reduction methods and a high fineness ratio.
- High-strength, low-weight, and heat-resistant materials such as high-strength aluminum must be used in missile replacement construction.
- The Missile body must have a high fineness ratio and low drag for optimum performance with respect to angle of attack and Mach number.

- The radar cross-section can be improved in tandem with volumetric efficiency to decrease detectability.
- Flares should not be used on the AIM-120 to improve stability.
- The aspect ratio for both the wings and tail should be kept low to ensure performance.
- Further military grade metals be researched to find the best possible metal to make the inflatable ducts out of.

7.3 Section Responsibilities

- **James Wall** – Worked on sections 4, 5, and 6. We evenly distributed the workload amongst ourselves to keep responsibilities reasonable.
- **Niels Braaten** – Worked on sections 4, 5, and 6. We evenly distributed the workload amongst ourselves to keep responsibilities reasonable.
- **Sap Dutta** – Worked on sections 3, 4, and 5. We evenly distributed the workload amongst ourselves to keep responsibilities reasonable.
- **Charlie Platt** – Worked on sections 1, 2, and 6. We evenly distributed the workload amongst ourselves to keep responsibilities reasonable.
- **Isaac Larsen** – Worked on sections 2, 3, and 6. We evenly distributed the workload amongst ourselves to keep responsibilities reasonable.

References

- [1] J. Wall and e. al., "RAIDER AIM-120 Replacement," 2023.
- [2] D. R. M. Barrett, "2023_Air_Armament_Symposium," November 2023. [Online]. Available:
https://drive.google.com/drive/folders/17QtHS0pAuUc9lei_uBrMICFYkNDcV_FO.
[Accessed 20 November 2023].
- [3] E. L. Fleeman, Missile Design and System Engineering, Lilburn: American Institute of Aeronautics and Astronautics, Inc, 2012.
- [4] J. Anderson, Fundamentals of Aerodynamics, New York: McGraw-Hill Education, 2017.
- [5] Anon., "Maraging Steel C-300 | T-300," Alloys International, Inc., [Online]. Available:
<https://alloysintl.com/inventory/alloys-steels-supplier/maraging-steel-300/>.
- [6] Anon., "3.125" Maraging Steel Round Bar 250-Annealed," OnlineMetals, [Online]. Available: <https://www.onlinemetals.com/en/buy/alloy-steel/3-125-maraging-steel-round-bar-250-annealed/pid/12619>.
- [7] Anon., "ALLOY X750 / INCONEL X750," Corrotherm International, [Online]. Available: <https://www.corrotherm.co.uk/grades/inconel-alloy-x-750>.
- [8] Anon., "INCONEL X-750 PLATE," Altemp Alloys, [Online]. Available: <https://www.altempalloys.com/inconel-x-750-plate.html>.
- [9] Anon., "Nitinol technical properties," Johnson Matthey, [Online]. Available: <https://matthey.com/en-US/products-and-markets/other-markets/medical-components/resource-library/nitinol-technical-properties>.
- [10] Anon., "Daily Metal Spot Prices," Daily Metal Prices, [Online]. Available:
] <https://www.dailymetalprice.com/metalprices.php?c=ni&u=lb&d=20>. [Accessed 2 December 2023].
- [11] Anon., "Titanium, Ti," MatWeb, [Online]. Available:
] <https://www.matweb.com/search/DataSheet.aspx?MatGUID=66a15d609a3f4c829cb6ad08f0dafc01&ckck=1>.
- [12] Anon., "How much is titanium worth per pound?," The Money, [Online]. Available:
] <https://themoney.co/how-much-is-titanium-worth-per-pound/>.
- [13] Anon., "AIM-120 AMRAAM," Military Today, [Online]. Available:
] https://www.militarytoday.com/missiles/aim120_amraam.htm. [Accessed 10 September 2023].

[14 D. J. Roskam, Airplane Aerodynamics and Performance, Lawrence, Kansas: Design,
] Analysis and Research Corporation (DARcorporation), 1997.